Non-destructive evaluation of resistance projection welded joints (RPW) by flash thermography

Non-destructive evaluation of resistance projection welded joints (RPW) by flash thermography

G. Dell'Avvocato[*], D. Palumbo[*], R. Pepe[**], U.Galietti[*]

[*]Polytechnic University of Bari – Department of Mechanics, Mathematics and Management – Via Orabona, 4 – 70125, Bari – Italy
[**]CRF/WCM R&I, Campus Manufacturing, Zona Industriale San Nicola di Melfi, 85025 Melfi (Pz), Italy

giuseppe.dellavvocato@poliba.it

Abstract. Pulsed thermography is a well-known thermographic method used as non-destructive control for detecting defects and evaluating the quality of components. One of the most challenging application is the development of thermographic non-destructive methods on thin welds for quality control, in order to overcome the limits of commons non-destructive methods such as ultrasound tests (UT). In the present work, pulsed thermography in reflection mode with flash lamps excitation, post-processed by pulsed phase thermography (PPT), has been used on resistance projection welded joints (RPW). A set of RPW specimens has been produced according to a factorial plan and a procedure to identify welding parameters by analysing the phase profile has been developed. The results have been analysed by using the ANOVA and the features extracted have been verified.

1. Introduction

In the automotive industries, resistance welding is very common, especially for joints in bodywork*[1,2,4–8]*. One of the most critical aspects related to the use of welded joints in industries is the possibility to carry out a quality control that, usually, is performed by traditional standard destructive methods as peeling test or chisel test (ISO10447). Another way to control the quality of the joints in the industrial field is by ultrasound (UT) non-destructive techniques *[9,10]*. These methods are well established but there are limits: the control is based on a statistical approach, time-consuming tests, the contact between the probe and specimen is required, difficult for thin materials and expansive automatization.

Pulsed thermography (PT) allows for overcoming the limits described above and has many advantages over the techniques described above, as the possibility to full-field control, no contact with specimen or component, the possibility to control the 100% of products, faster than ultrasounds method and, unlike the latter, it can be easily automated *[1,2,4]*.

Pulsed thermography, based on thermal wave theory *[11,12]*, consists in the thermal excitation of a sample by means of a thermal pulse (Dirac) and then analyzing the cooling or heating transient because, if there is a defect, there will be a different behavior of the material, due to the different thermophysical characteristics of the defective area compared to the non-defective one, which will allow the detection of the defect. Thickness variations can also be detected using the same approach and set-up.

The thermal field on the surface is recorded by an IR camera and a thermal sequence is acquired during the cooling phase of the material. If the inspected surface is the same that has been excited by a heat source, it is called *reflection mode set-up*; otherwise, if the observed surface is the opposite one to the thermally excited one, it is called *transmission mode set-up.*

In literature, there are several applications of pulsed thermography for detection and quantification of defects in composites and in metals *[3,13–19]*. Often, thermal images are not sufficient for a good evaluation of data and post-processing algorithms are needed for improving the signal to noise ratio. In the present work, the pulsed phase thermography (PPT) *[3]* algorithm has been used, and the phase maps have been analyzed.

Thermographic non-destructive techniques applied on the resistance welded joints, in particular resistance spot-welded joints (RSW), are present in literature for two different configurations: transmission *[1]* and reflection mode *[2].*

In the present work, resistance projection (RPW) welded joints have been investigated. In the RPW two plates are forced in contact between two electrodes, exactly the same that RSW. The main difference with respect to the RSW process is that in the RPW one the plates have embossing that allows for increasing the resistance for the current flow and, consequently, reducing the applied force, the processing time and the current to obtain the welding. Moreover, more localized heating is obtained that reduce the heat-affected zone (HAZ) because the temperature developed is higher than in RSW but in the smallest area *[24-25] Fig.1.* Moreover, the RPW joints present a very smooth surface that makes it suitable for aesthetic applications, especially for the automotive industries.

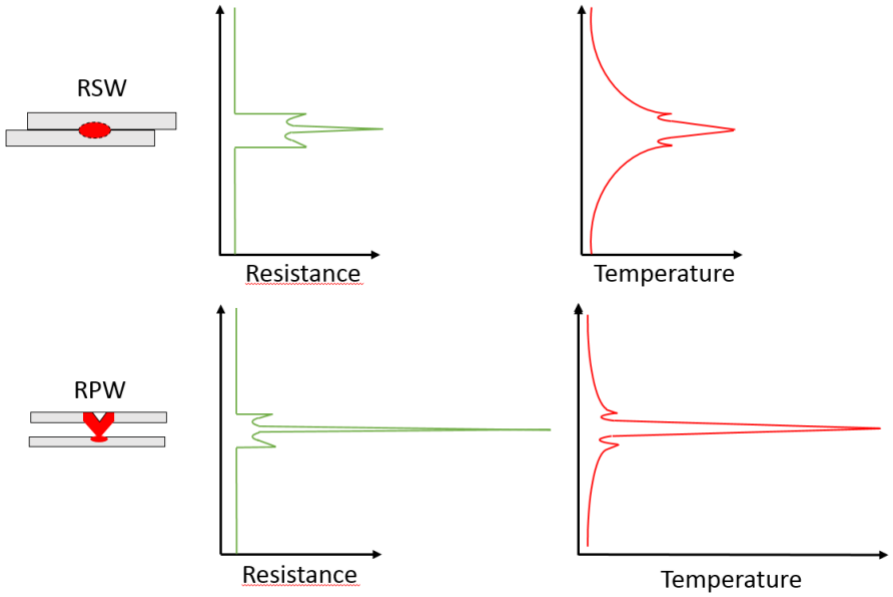

Figure 1. Scheme of difference between RSW joints and RPW joints. Green curves show the resistance as function of the distance from the contact area. Red curve shows the temperature distribution in depth direction during the welding process.

In Fig. 2 is possible to see the geometry of investigated joints that shows the rectangular shape of embossing and also the side of the welded joint without embossing that has no particular scratches as instead are visible in RSW joints *[24-25].*

In the present work, the aim is to develop a thermographic NDT procedure to allow the quality inspection of RPW joints, in particular, to identify process welding parameters by pulsed thermography after the application of PPT algorithm.

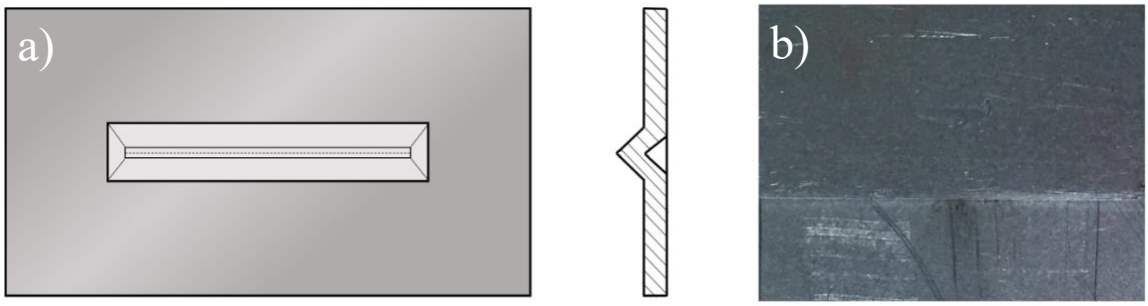

Figure 2. (a) Embossing geometry for the inspected resistance projection welding (RPW) (b)Front surface of joints without paint.

2. Theory

Active pulsed thermography considers a solution of heating transmission equation in the hypothesis of Dirac pulse, semi-infinite body, unidimensional flux, homogeneous and isotropic body, adiabatic process *[11,12]*.

$$T(z,t) = T_0 + \frac{Q}{\sqrt{k\rho C\pi t}} exp^{-\frac{z}{4\alpha t}} \quad (1)$$

The equation above is written at depth *z,* for a body with thermal diffusivity α, with density ρ, thermal conductivity *k*, heat capacity *C*, at time *t* that is the instant after heat pulse. For a reflection mode set-up, the temperature on the surface (*z=0*) can be written below with $e=\sqrt{k\rho C}$ that is thermal effusivity:

$$T(0,t) = T_0 + \frac{Q}{e\sqrt{\pi t}} \quad (2)$$

2.1. Pulsed phase thermography

Pulsed phase thermography (PPT) is one of the most known algorithm based on the principle that every signal, can be decomposed in single components: each one at a different frequency and with different amplitude *[3,20,21].* To analyse the signal in the frequency domain, the Fourier transform is used. Precisely, it is not possible to apply the continuous Fourier transform (CFT) because the thermal signal recorded by the IR camera is a discrete signal, so the Discrete Fourier Transform (DFT) is used *[3,20,21].*

$$F_n = \Delta t \sum_{k=0}^{N-1} T(k\Delta T) e^{-\frac{i2\pi nk}{N}} = Re_n + Im_n \quad (3)$$

In the equation above, *n* is the increment of frequency but one important term that must be considered is Δt that is the sampling interval. This term is very important in order to reduce the difference between CFT and DFT *[3].* Usually, for the evaluation of DFT, a well-known algorithm is used that is the Fast Fourier Transform that reduces computational work to a factor $(N \log N)$ *[22].*
Phase and amplitude for each frequency can be obtained in order to have two 3D matrices where there are frequencies on one axes and, respectively, phase and amplitude for each pixel *[3,20,21].*

$$A_n = \sqrt{Re_n^2 + Im_n^2} \qquad \phi_n = arctg\left(\frac{Im_n}{Re_n}\right) \quad (4)$$

Since thermal profile are *Hermite function* because the real part is even but the complex part is odd, in the frequency domain, phase and amplitude are equal and odd; in fact, for a thermal sequence with N thermograms, phase and amplitude matrix have only $^{N}/_{2} + 1$ useful frequencies.
It is important to understand that, the resolution in the time domain is defined by acquisition frequency because the value of Δt is determined as follow:

$$\Delta t = \frac{1}{f_s} \quad (5)$$

In the frequency domain the resolution it is connected to the length of the signal in the time domain: in fact, the value of Δf is:

$$\Delta f = \frac{1}{N\Delta t} = \frac{1}{w(t)} \quad (6)$$

This is the reason why the length of time window it is not important only for the description of thermal signal from the back wall of the specimen, but also to improve the resolution in the frequency domain that is important because the frequency of excitation is related to the depth inspected as written below where: α is thermal diffusivity, z is the depth and f the frequency of thermal excitation *[3,20,21]*.

$$z \propto \sqrt{\frac{\alpha}{\pi f}} \quad (7)$$

3. Materials and methods

3.1. Samples

In the present work, 12 samples with the same geometry were investigated. The specimens analyzed have the embossed plate made in FeP04 (0.67 mm) and the smooth plate in FeP05 (0.70 mm), joined by resistance projection welding. The rectangular emboss measure 9 mm x 1.2 mm as shown in *Fig. 3*.

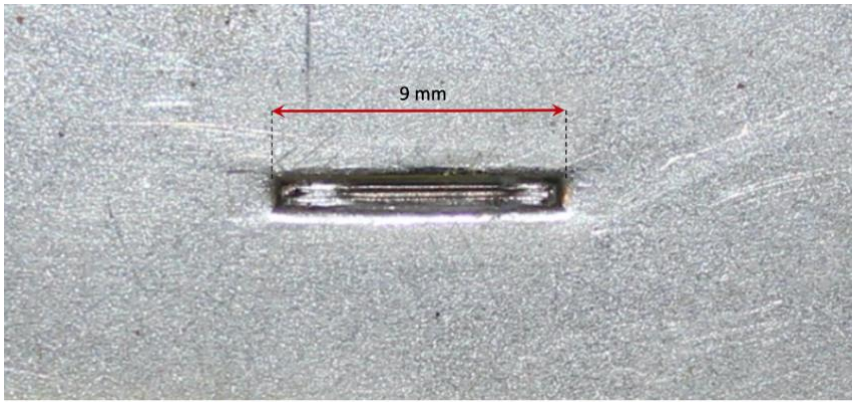

Figure 3. Picture of one of the embossing on the investigated specimens (rear surface).

In order to evaluate the simultaneous effects of the welding parameters on the joint and the interactions among them, it was used a factorial plan. The obtained Design Of Experiment (DOE) technique allows us to save time and reduce the total number of experiments compared with the traditional procedure where the welding parameters are changed one by one. In the proposed DOE there are 3 parameters that changes (F, I, t) with 2 levels for each one for a sum of 4 sets of parameters. To evaluate the repeatability of the process too, 3 replications for each set of parameters are obtained, so the total number of specimens was 12.

Unlike RSW, where the surface of the welded joint has the same characteristics on both sides, in RPW, one of the plates is embossed, so it is possible to define front side and rear side. The rear side is where the embossed plate is the first, so it is evident the shape of the electrode, the front side is the plate without embossing and where the surface is completely smooth. This aspect is very important because, in the applications of thermography to RSW joints, one of the critical aspects is the difference of emissivity in the welded spot that generates a difference in the signal recorded by IR camera that not correspond to a real difference of temperature, so it is necessary to compensate this phenomenon. To avoid the influence of emissivity, especially to avoid the difference in absorbed energy, a thin paint layer with high known emissivity has been used to cover the specimen surfaces.

Table 1. Specimen welding parameters description.

Sample	(I) Current (kA)	*(F) Force (kN)*	(t) Time (ms)	*Replications*
J1_DOE_1	15	1.4	10	3
J1_DOE_2	13	1.4	12	3
J1_DOE_3	13	1.6	10	3
J1_DOE_1	15	1.6	12	3

3.2. Set-up

The experimental set-up is showed in Fig.4. The reflection mode was used because less space than transmission mode is needed, so can fit and better reproduce an industrial application and because the front surface is smooth and guarantees uniform heat absorption.

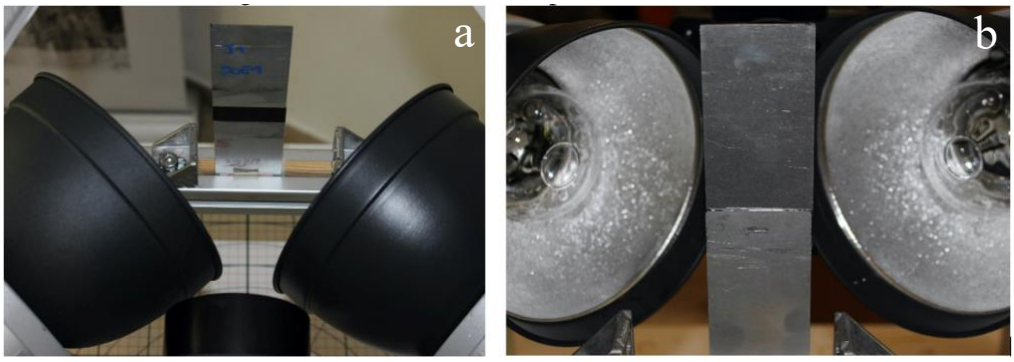

Figure 4. Experimental set-up in reflection configuration. (a) The front surface of specimen with black coating. (b) The back surface of specimen with embossing.

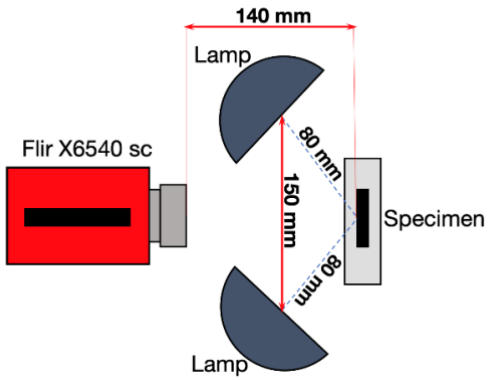

Figure 5. Schematic representation of experimental set-up used.

Two flash lamps (Hensel HP Pro 3000 J) have been used for the pulse heating with a pulse time duration of ~3 ms that is a good approximation for an instantaneous excitation (Dirac function); 5 s after heating pulse have been recorded. As it is possible to see in the diagram of experimental set-up in Fig.5, the specimen is in the middle of two lamps and in front of IR camera (FLIR X6540 sc) and the distance of 140 mm between IR camera lens and specimen were measured. To have a good spatial resolution, it is necessary to have more pixel as possible on the region of interest (ROI) and it is good to put the IR camera closer as possible to the specimen, so a lens 50 mm with 12 mm extension ring has been used to have an mm/pixel ratio of 0.055 mm/pixel. On the other hand, to have a good time resolution and describe as well as possible the phenomena, as the cooling down of metal specimen after pulse heating, a high frame rate is needed. To achieve the frame rate of 910 Hz, a reduced acquisition window has been chosen (304 x 104 pixels) with the integration time of 0.5650 ms.

For controlling the thermal excitation and synchronizing it with the IR Camera, the PC, flash lamps and the IR camera have been connected to the MultiDES System®, as is showed in *Fig.6.*

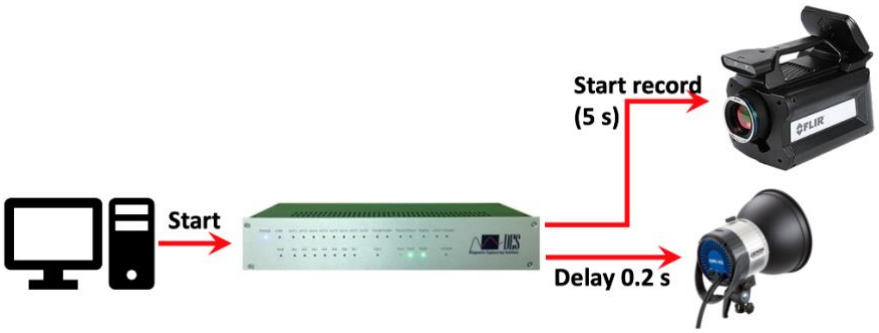

Figure 6. Scheme of system used for the experimental tests.

3.3. Methods

For each test, a thermographic sequence of 5 s has been recorded, that can be represented by a 3D matrix (x, y, t). For all thermographic sequences, the same operations have been carried out. First, a cold frame was subtracted to all the sequence in order to reduce background noise and the influence of the reflection. Then, after the identification of saturated thermograms, the early recorded thermogram (ERT) has been identified and the time axis was shifted to have at time 0 the ERT; frames before ERT has been neglected. On the thermographic sequence is needed to define the last recorded thermogram (LRT) that is strictly related to which frequency it is possible to have on the frequency axis (for phase and amplitude 3D matrix) and not only depends on the maximum depth that is needed to investigate. In fact, in the frequency domain, the maximum value of the frequency depends on the frame rate ($f_{max} = f_s/2$), but Δf depends on the number of elements between f_{min} and f_{max} that is $^{N}/_{2} + 1$, where $N = LRT - ERT$. For these reasons, it has been decided to use the same fixed number of thermograms in order to be able to have phase and amplitude 3D matrix with the same values of frequencies axis and to have the possibility to compare phase or amplitude maps at the same frequencies, therefore depth, for each test. Because of the characteristics of the fast Fourier transform (FFT) algorithm, $N = 4096$ has been chosen because if $N = 2^k$, $\mathcal{O}(N \log_2 N)$ operations are needed instead of $\mathcal{O}(N^2)$.

By using the MATLAB® software, the algorithm of PPT has been applied, which has provided two 3D matrices: one for amplitude and one for phase. Attention has been focused mainly on phase matrix because is less influenced by reflection problems and inhomogeneous heating problem.

In order to evaluate the quality of the joints, and then identify characteristics that are related to the process parameters, it was decided to analyze the trend of the phase signal along a profile passing through the center of the embossing, then the welding. The profile has been selected starting to the rear side where the embossing is clearly visible, considering a line ~12 mm long, passing through the

center of the embossing (9 mm long), as shown in the Fig.7. To reduce the noise of the signal, an average among 3 lines for 216 pixels has been considered: the pixel array passing through the center of the embossing and the pixel arrays just above and just below. The value of the first element of the array has been subtracted to all other values of the array, for each phase profile extracted. This procedure allows us to have for all profiles *"0"* as the first value and the comparison among results.

To carry out the analysis of the factorial plan by ANOVA, it is needed to identify "features" that will permit to quantify the difference among the phase profiles. Two features have been extracted from the phase profile: the minimum value of phase and the slope of profile in the first part, as it is possible to see in Fig. 8. A second-order polynomial fitting has been applied to obtain the value of minimum in the profile. In particular, about 70 data have been considered for each profile. From the polynomial equation, the value of the minimum has been calculated. For the second feature, 30 pixels (from 37 to 67) has been considered and a first-order polynomial and the value of angular coefficient has been used as the second feature to quantify the slope of that part of phase profile.

The ANOVA has been performed to investigate the dependence among the features and the welding process parameters since in this way, it is possible to understand if the difference among the value of features can be attributed to the difference of welding parameters or not.

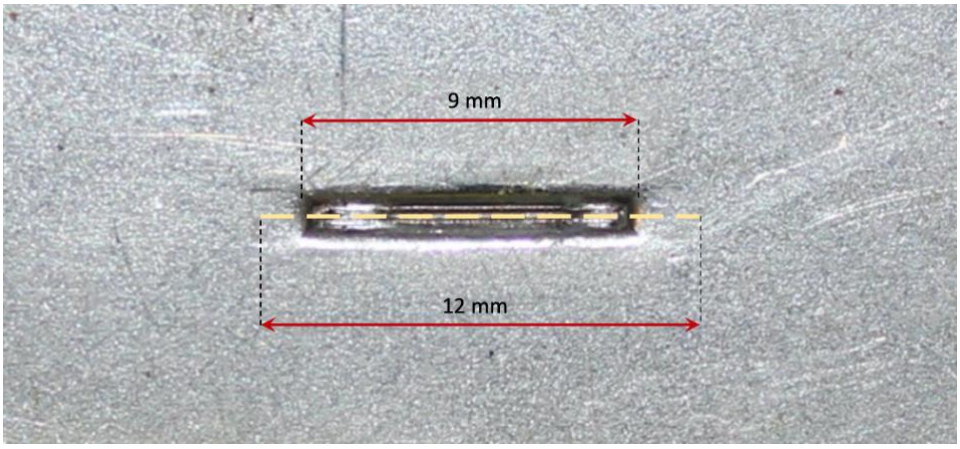

Figure 7. In yellow it is represented the line considered for the profile selection with length 12 mm.

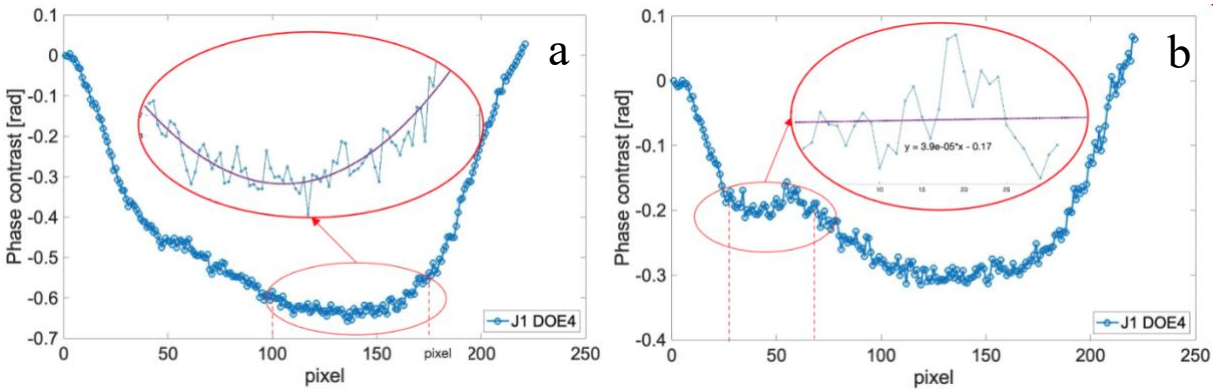

Figure 8. In the pictures it is showed the features selection. To the (a) Phase profile for f=0.444 Hz and the selection of minimum between pixels 100 and 170. (b) Phase profile for f=4.884 Hz and selection of value of slope between pixels 37 and 67.

4. Results and discussion

Thermographic results do not show a symmetric thermal map along the weld from left to right, Fig. 9. In fact, immediately, by thermographic images, it is possible to see that the signal in the left part of thermogram is different from the right side. Observing the welding from the rear side, it is possible to see that the embossed plate is not perfectly symmetric and this could be caused by not perfect contact between the smooth plate and embossed part and for a non-homogeneous distribution of force for all the length of embossing. It is reasonable to think that, during the process, the heat follows the current flow that starts to go through the plate from the part of embossing in contact and in the part of the surface with a minimum radius of curvature.

As written above in section 3.3, the thermographic sequence has been post-processed by the PPT algorithm, especially to reduce the noise that is present in the thermal image, as it is shown in *Fig. 9*. In fact, in *Fig.9 (a)* there is a thermal image after the cold frame subtraction, and it is possible to see that the signal is noisy, and some paint spots are visible as hot spots.

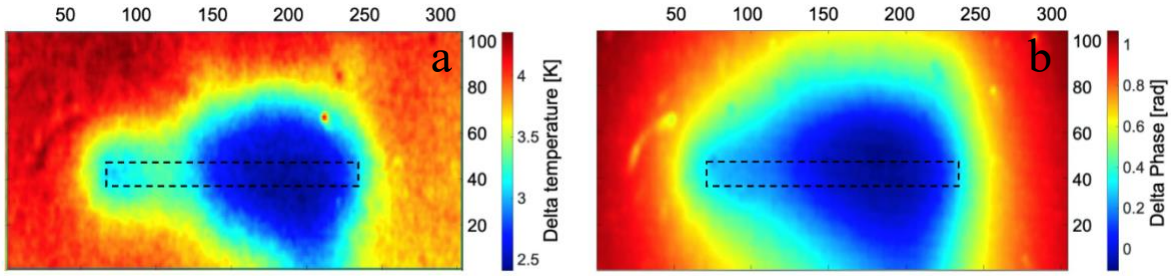

Figure 9. (a) Thermal image for the DOE_1_A at t=27.5 ms after the ERT. (b) after the application of PPT algorithm, phase image for f=0.444 Hz for DOE_1_A.

In *Fig.9 (b)*, it is possible to see a phase map that corresponds at the same test showed in *Fig.9 (a)* but, the phase image is sharper than the thermal one, less noisy and that the hot spot is not visible. The reason why the hot spot disappears is that the phase image in *Fig. 9 (b)* corresponds to a low frequency, then to a high depth section; in addition, usually, the phase map obtained by PPT is lower influenced by non-uniform heating *[3,20,21,23]* and for this motivation is used more than amplitude data.

For the first 25 frequencies (from 0.444 Hz to 10.108 Hz), as described in section 3.3, phase profiles have been considered and four of them are shown in *Fig.10 (a)*, each one correspondent to a different set of welding parameters (F, I, t) for the frequency 0.444 Hz. It is possible to see in *Fig.10 (a)* that the profiles have the same behaviour but there is a shift among the curves and the difference among the value of an absolute minimum of the profile curve, can be used to distinguish curves, then welding parameters. In *Fig.10 (b)* are shown four profiles but for a higher frequency of 4.884 Hz, that means closer to the surface than the profiles in *Fig.10 (a)*. For the high frequency, the value of the minimum of the curve, that for low frequencies shows the difference among different specimens, has no relevant difference but, the behaviour of the profiles is different, especially in the first part of profile where the profiles seem to have 2 different behaviours: DOE_1 and DOE_2 shows a different slope from DOE_3 and DOE_4.

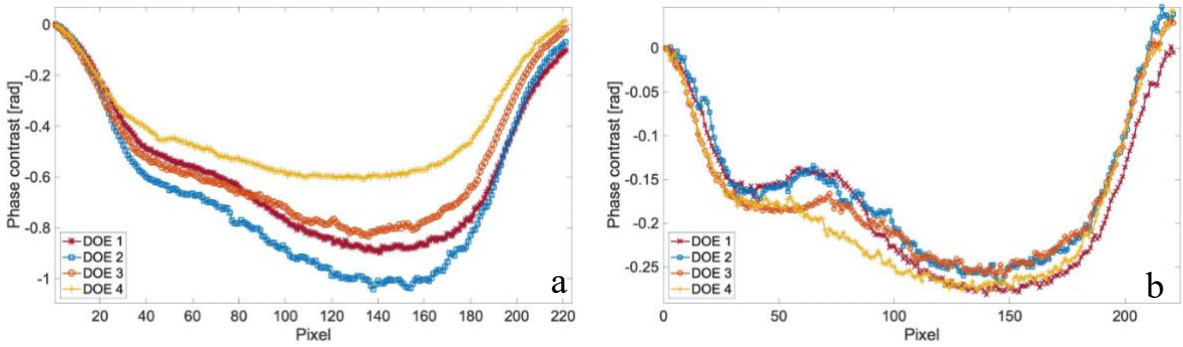

Figure 10. (a) Phase profile for different DOE at f=0.444 Hz and (b) at f=4.884 Hz.

The values of minimum (P_1) has been assessed for the first 25 frequencies between pixel 100 and 170, while the slope values (P_2) between pixel 37 and 67, as described in section 3.3. For each frequency, the ANOVA was performed for both indexes P_1 and P_2 and the confidence level was fixed to 95%. In *Table 2*, the values of P1 and P2 for each specimen, for the most significant frequencies, are reported. These two frequencies (0.444 Hz and 4.884 Hz) were chosen because they are the two frequencies for which the parameters investigated showed higher significance, therefore P-value lower. The Pareto diagrams in *Fig.11(a)* shows at frequency 0.444 Hz that the value of P_1 is influenced by the force (F) and the current (I) but only for low frequencies; in fact, results show no significance for higher frequencies. In *Fig.11(b),* the Pareto diagram for high frequency has been reported: it shows that the value of P_2, that for lower frequency has no dependence on welding parameters, at high frequencies depends on the value of the force. It is interesting that that dependence of P_2 from F starts to be significative from frequency *f=5.332 Hz* until frequency *f=10.220 Hz*, and this could be useful for optimization of PPT parameters. There is no parameter that shows a dependence from *t* but does not mean that there is not. In fact, in developing a factorial plan, it is very important the choice of values used for the two levels of parameters, because, if the values are very close could be possible that the influence on the process it is not strong enough to be detected. The values of time in welding parameters are 10 ms and 12 ms, which are very close, but the confirmation of this hypothesis will be possible only after comparison with destructive standard testing.

Table 2. Values of minimum and slope for 2 frequencies f=0.444 Hz and f=4.884 Hz.

Sample	Current (kA)	*Force (kN)*	Time (ms)	*Min at 0.444 Hz*	*Slope at 0.444 Hz*	*Min at 4.884 Hz*	*Slope at 0.444 Hz*
J1_DOE_1_A	15	1.4	10	-0.891	-33.03 E-04	-0.306	11.08 E-04
J1_DOE_1_B	15	1.4	10	-0.735	-28.02 E-04	-0.262	9.616 E-04
J1_DOE_1_C	15	1.4	10	-0.696	-29.19 E-04	-0.263	6.571 E-04
J1_DOE_2_A	13	1.4	12	-0.900	-34.13 E-04	-0.268	1.681 E-04
J1_DOE_2_B	13	1.4	12	-0.881	-26.34 E-04	-0.218	7.228 E-04
J1_DOE_2_C	13	1.4	12	-0.788	-11.26 E-04	-0.287	22.68 E-04
J1_DOE_3_A	13	1.6	10	-0.766	-29.09 E-04	-0.313	-1.878 E-04
J1_DOE_3_B	13	1.6	10	-0.687	-25.56 E-04	-0.210	4.038 E-04
J1_DOE_3_C	13	1.6	10	-0.645	-23.34 E-04	-0.239	-0.620 E-04
J1_DOE_4_A	15	1.6	12	-0.544	-16.51 E-04	-0.226	-10.59 E-04
J1_DOE_4_B	15	1.6	12	-0.560	-31.95 E-04	-0.327	-7.739 E-04
J1_DOE_4_C	15	1.6	12	-0.603	-23.37 E-04	-0.260	0.387 E-04

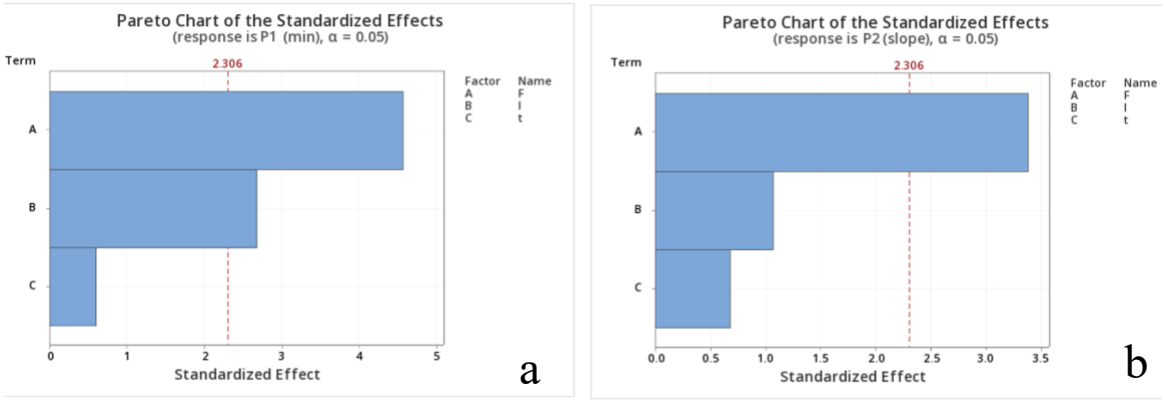

Figure 11. (a) Pareto chart of the standardized effects for values of minumum at f=0.444 Hz. (b) Pareto chart of the standardized effects for values of slope at f=4.884 Hz.

Table 3. Analysis of Variance for value of minimum at f=0.444 Hz.

Source	Seq SS	*Contribution*	Adj SS	*Adj MS*	*F-Value*	*P-Value*
Model	0.133606	77.93 %	0.133606	0.044535	9.41	0.005
Linear	0.133606	77.93 %	0.133606	0.044535	9.41	0.005
F	0.098051	57.19 %	0.098051	0.098051	20.73	0.002
I	0.033825	19.73 %	0.033825	0.033825	7.15	0.028
t	0.001730	1.01 %	0.001730	0.001730	0.37	0.562
Error	0.037845	22.07 %	0.037845	0.037845		
Total	0.171451	100 %	0.171451			

Table 4. Analysis of Variance for value of slope at f=4.884 Hz.

Source	Seq SS	*Contribution*	Adj SS	*Adj MS*	*F-Value*	*P-Value*
Model	0.000005	61.87 %	0.133606	0.044535	4.33	0.043
Linear	0.000005	61.87 %	0.133606	0.044535	4.33	0.043
F	0.000005	54.24 %	0.098051	0.098051	11.38	0.010
I	0.000000	5.43 %	0.033825	0.033825	1.14	0.317
t	0.000000	2.20 %	0.001730	0.001730	0.46	0.516
Error	0.000003	38.13 %	0.037845	0.037845		
Total	0.000009	100 %	0.171451			

5. Conclusions

In the present work active thermography has been applied to resistance projection welding joints, in order to evaluate the quality of the joint and to find a thermographic NDT procedure that can be used to identify welding parameters by thermographic features.

To find these features, a well-established algorithm has been used that is the pulse phase thermography and profiles on phase maps have been analysed. It was demonstrated that the pulsed thermography can be used for the evaluation of projection resistance welded joint.

Phase maps for the first 25 frequencies have been analysed and the frequencies that maximize results were chosen (0.444 Hz – 4.448 Hz) but probably will be possible to optimize the parameters used for PPT algorithm. Two different indexes that can give information about current (I) and force (F) used in the welding process were identified and the ANOVA has been performed. Results showed that is possible to recognize two of three welding parameters, with a confidence of 95%. In fact, in the

phase contrast profile, the value of min at low frequencies (P_1) and the slope in the first part of welding (P_2) at higher frequencies, are sensitive to the variation of current and force. The considered indexes give information about the two welding parameters (I, F) at different frequencies because they depend on different depths.

Time seems to have no influence on the features P_1 and P_2 but might be due to a too narrow time range chosen but, it can be confirmed only after traditional destructive standard tests.

Next steps for the present work are:

- To assess the mechanical characteristics of welded joints with destructive traditional test in order to relate them to welding parameters;
- Optimize the developed procedure to be able to maximise results and reduce computational work more as possible;
- To perform the developed NDT procedure without coating to validate the method on as is joints;
- Apply method to thicker specimens in order to verify that this technique can be applied, and which are the limits.
- Apply different algorithms in order to find new features and evaluate which is more convenient to use depending on applications.

Acknowledgements
This work has supported by Centro Ricerche Fiat WCM R&I, Campus Manufacturing with particular support of Mr Stefano Capobianco.

References

[1] Palumbo D, D'Accardi E and Galietti U 2019 A new thermographic procedure for non-destructive evaluation of RSW joints *Proc. SPIE Thermosense: Thermal Infrared Applications* **11004**

[2] Joinietz F, Myrach P, Suwala H and Ziegler M 2016 Examination of Spot Welded Joints with Active Thermography *J. Nondestruct. Eval.* ***35*** 1

[3] Ibarra-Castanedo C 2015 Quantitative Subsurface Defect Evaluation by Pulsed Phase Thermography *Doctorate Thesis Université Laval*

[4] Schlichting J, Brauser S, Pepke L A, Maierhofer C, Rethmeier M and Kreutzbruck M 2012 NDT & E International Thermographic testing of spot welds *NDT & E Int*. **48** 23–29

[5] Ambroziak A and Korzeniowski M 2010 Using resistance spot welding for joining aluminium elements in automotive industry *Arch. Civ. Mech. Eng.* **10** 5-13

[6] Pouranvari M and Marashi S P H 2013 Critical review of automotive steels spot welding: Process, structure and properties *Science and Technology of Welding and Joining* **18 (5)** 361-403

[7] Zhang H and Senkara J 2005 *Resistance welding: Fundamentals and applications* (London: Taylor & Francis CRC Press)

[8] Lee S, Nam J, Hwang W, Kim J and Lee B 2011 A study on integrity assessment of the resistance spot weld by infrared thermography *Procedia Eng.* **10** 1748–1753

[9] Summerville C, Adams D, Compston P and Doolan M 2017 Nugget Diameter in Resistance Spot Welding: A Comparison between a Dynamic Resistance Based Approach and Ultrasound C-scan *Proc. Eng.* **183** 257–263

[10] Summerville C, Compston P and Doolan M 2019 A comparison of resistance spot weld quality assessment techniques *Proc. Manuf.* **29** 305–312

[11] Maldague X, Galmiche F and Ziadi A 2002 Advances in pulsed phase thermography *Infr. Phys. & Techn.* **43** 175–181

[12] Carslow H S, Jaeger J C and Morral J E 1986 *Conduction of Heat in Solids Second Edition* (USA: Oxford University Press)

[13] Shepard S M 2003 Reconstruction and enhancement of active thermographic image sequences *Opt. Eng.* **42** 5

[14] Balageas D L, Roche J M, Leroy F H, Liu W M and Gorbach A M 2015 The thermographic signal reconstruction method: A powerful tool for the enhancement of transient thermographic images *Biocybern. Biomed. Eng.* **35** 1–9

[15] Palumbo D and Galietti U 2017 Thermal methods for evaluating flaws in composite materials: A new approach to data analysis *Conf. Proc. of the Society for Exp. Mech. Ser.* **7** 267-265

[16] Palumbo D and Galietti U 2016 Damage Investigation in Composite Materials by Means of New Thermal Data Processing Procedures *Strain* **52** 267-285

[17] Müller J P, Dell'Avvocato G and Krankenhagen R 2020 Assessing overload-induced delaminations in glass fiber reinforced polymers by its geometry and thermal resistance *NDT E Int.* ***116***

[18] Vavilov V P and Burleigh D D 2015 Review of pulsed thermal NDT : Physical principles , theory and data processing *NDT E Int.* **73** 28–52

[19] D'Accardi E, Palumbo D, Tamborrino R and Galietti U 2018 A Quantitative Comparison Among Different Algorithms for Defects Detection on Aluminum with the Pulsed Thermography Technique *Metals (Basel)* **8** 859

[20] Ibarra-Castanedo C and Maldague X P V 2005 Interactive methodology for optimized defect characterization by quantitative pulsed phase thermography *Res. Nondestruct. Eval.* **16** 175–193

[21] Ibarra-Castanedo C and Maldague X 2004 Pulsed phase thermography reviewed *Quant. Infrared Thermogr. J.* **1** 47–70

[22] Press W H, Flannery B P, Teukolsky S A and Vetterline W T 1990 12 . 2 Fast Fourier Transform (FFT) *Numerical Recipes: The Art of Scientific Computing* **1**

[23] Maldague X P, Ibarra-Castanedo C, Bendada A, González D and Galmiche F 2006 Discrete signal transforms as a tool for processing and analyzing pulsed thermographic data *Thermosense* **XXVIII 6205** 14

[24] European Patent n. EP 1 932 614 A1 (2008)

[25] European Patent n. EP 1 847 349 B1 (1999)